Atmospheric correction of optical imagery from MODIS and Reanalysis atmospheric products

Juan C. Jiménez-Muñoz, José A. Sobrino *, Cristian Mattar, Belen Franch

Global Change Unit, Image Processing Laboratory, University of Valencia, P.O. Box 22085, E-46071 Valencia, Spain

A B S T R A C T

In this paper we analyze the differences obtained in the atmospheric correction of optical imagery covering bands located in the Visible and Near Infra-Red (VNIR), Short-Wave Infra-Red (SWIR) and Themal-Infrared (TIR) spectral regions when atmospheric profiles extracted from different sources are used. In particular, three sensors were used, Compact High Resolution Imaging Spectrometer (CHRIS), Advanced Spaceborne Thermal Emission and Reflection radiometer (ASTER) and Landsat5 Thematic Mapper (TM), whereas four atmospheric profiles sources were considered: i) local soundings launched near the sensor overpass time, ii) Moderate Resolution Radiometer (MODIS) atmospheric profiles product (MOD07), iii) Atmospheric Correction Parameter Calculator (ACPC) generated by the National Center for Environmental Prediction (NCEP) and iv) Modified Atmospheric Profiles from Reanalysis Information (MAPRI), which includes data from NCEP and National Center of Atmospheric Research (NCAR) Reanalysis project but interpolated to 34 atmospheric levels and resampled to 0.5°×0.5°. MODIS aerosol product (MOD04) was also used to extract Aerosol Optical Thickness (AOT) values at 550 nm. Analysis was performed for three test dates (12th July 2003, 18th July 2004 and 13th July 2005) over an agricultural area in Spain. Results showed that air temperature vertical profiles were similar for the four sources, whereas dew point temperature profiles showed significant differences at some particular levels. Atmospheric profiles were used as input to MODTRAN4 radiative transfer code in order to compute atmospheric parameters involved in atmospheric correction, with the aim of retrieving surface reflectances in the case of VNIR and SWIR regions, and Land Surface Temperature (LST) in the case of the TIR region. For the VNIR and SWIR region, significant differences depending on the atmospheric profile used were not found, particularly in the Visible region in which the AOT content is the main parameter involved in the atmospheric correction. In the case of TIR, differences depending on the atmospheric profile used were appreciable, since in this case the main parameter involved in the atmospheric correction is the water vapor content, which depends on the vertical profile. In terms of LST retrieval from ASTER data (2004 test case), all profiles provided satisfactory results compared to the ones obtained when using a local sounding, with errors of 0.3 K for ACPC and MAPRI cases and 0.7 K for MOD07. When retrieving LST from TM data (2005 test case), errors for MOD07 and MAPRI were 0.6 and 0.9 K respectively, whereas ACPC provided an error of 2 K. The results presented in this paper show that the different atmospheric profile sources are useful for accurate atmospheric correction when local soundings are not available. In particular, MOD07 product provides atmospheric information at the highest spatial resolution, 5 km, although its use is limited from 2000 to present, whereas MAPRI provides historical information from 1970 to present, but at lower spatial resolution.

© 2010 Elsevier Inc. All rights reserved.

1. Introduction

The removal of the atmospheric perturbation introduced in the signal registered by remote sensing sensors is one of the key elements in order to obtain accurate geo/biophysical products for Earth observation purposes. The relationship between Top of Atmosphere (TOA) signal and Top of Canopy (TOC) or ground-level signal is given by the Radiative Transfer Equation (RTE), written in different forms depending on the spectral range considered. Hence, when working in the Visible and Near Infra-Red (VNIR) and Short-Wave Infra-Red (SWIR) spectral ranges, both absorption and scattering processes should be accounted for, whereas when working in the Thermal Infra-Red (TIR) range scattering processes are commonly neglected and only atmospheric absorption is considered.

In general terms, conversion from TOA to TOC (or ground-level) signal is referred as Atmospheric Correction or Atmospheric

* Corresponding author.
E-mail addresses: jcjm@uv.es (J.C. Jiménez-Muñoz), sobrino@uv.es (J.A. Sobrino).

Compensation (AC). This conversion is not totally direct in the case of TIR data, since once the radiance at ground-level (or land-leaving radiances) is obtained, there is still an atmospheric contribution in it, due to the coupling between atmospheric down-welling radiance and surface emissivity. In the case of the VNIR/SWIR range, it is possible to obtain a TOC signal free of atmospheric effects, both in radiance units as well as reflectance units. In any case, when this conversion is achieved directly from inversion of the RTE, one needs to compute the different atmospheric parameters involved. This requires the knowledge of vertical distribution for some meteorological variables, i.e., requires the availability of an atmospheric profile, which could be achieved by launching an atmospheric sounding. This information can be introduced into a Radiative Transfer Code (RTC) and then, after band averaging according to the system spectral response of a certain sensor band, retrieve the atmospheric parameters required for AC.

In this paper MODTRAN4 RTC code (Berk et al., 1999) has been used, since it represents the state of the art in realistic computing of absorption and scattering in the terrestrial atmosphere at high spectral solution ($1 \, \mathrm{cm}^{-1}$) over the VNIR, SWIR and TIR spectral ranges, providing accurate simulations of atmospheric radiative transfer (Guanter et al., 2009; Verhoef & Bach, 2003). MODTRAN includes the Discrete Ordinates Radiative Transfer code for a Multi-Layered Plane-Parallel Medium (DISORT) algorithm (Stamnes et al., 1988), which can be used for accurate multiple scattering calculations.

Dedicated calibration and validation activities are periodically carried out in the framework of different field campaigns organized by different agencies or institutions. These activities commonly include the launch of an atmospheric sounding near the overpass time of a certain sensor in order to perform accurate ACs. Since in most cases local soundings are not available, it is important to assess the feasibility of using other external sources of atmospheric profiles for accurate AC of optical imagery. This is the main purpose of this paper. In particular, the study focuses on profiles extracted from Moderate Resolution Radiometer (MODIS) Atmospheric profiles product (MOD07) and on profiles extracted from Reanalysis information, whose resolutions have been vertically and spatially improved in relation to other existing Reanalysis-based profiles. MOD07 products provide daily atmospheric profiles at 5 km spatial resolution and at world-wide scale since year 2000, thus providing a powerful information for AC of any kind of imagery, from high to low resolution ones. As far as we know, MOD07 is the existing atmospheric profiles product with the highest spatial resolution. Results will be analyzed for three test dates in the framework of different field campaigns carried out over an agricultural area, in which local atmospheric soundings were launched. MOD07 and Reanalysis-based vertical profiles were compared to local soundings, considered as the "ground-truth", and differences on the AC depending on the atmospheric profile used were analyzed. Satellite sensors included in this study were the Compact High Resolution Imaging Spectrometer (CHRIS) on-board the Project for On-Board Autonomy (PROBA) platform, the Advanced Spaceborne Thermal Emission and Reflection Radiometer (ASTER) on-board the TERRA platform, and Thematic Mapper (TM) on-board the Landsat-5 satellite.

The paper is organized as follows: Section 2 provides the theoretical basis for radiative transfer in the VNIR and SWIR spectral ranges, including description of methods for surface reflectance retrieval, whereas Section 3 provides the theoretical basis for radiative transfer in the TIR region, including description of methods for LST retrieval; Section 4 presents the test area and imagery used in the study, and Section 5 includes a description of the different atmospheric profiles sources considered in this paper; Section 6 shows the results obtained in the intercomparison of the different vertical profiles, and Section 7 shows the results obtained in the atmospheric correction in the VNIR/SWIR (reflectance retrievals) and TIR (LST retrievals) cases; finally, Section 8 summarizes and includes the main conclusions drawn from the study presented in this paper.

2. Theoretical basis for atmospheric correction in the VNIR and SWIR

Atmospheric correction in the VNIR and SWIR regions usually refers to the conversion of TOA radiances (or at-sensor radiances) into surface reflectances. In comparison to the TIR region (analyzed in the next section), the expression for the RTE in the VNIR/SWIR is probably subjected to more variations depending on the different assumptions considered. In this paper we will start from the RTE as presented in Verhoef and Bach (2003), which is based on a four-stream approximation and provides a complete description for the different contributions involved in the AC. Since this approach is not easy to implement for a non-experienced user, we will propose a simplified methodology based on MODDTRAN4 calculations which use MODTRAN outputs directly, and then a deep knowledge of radiative transfer issues is not required.

2.1. Four-stream land-atmosphere radiative transfer

The four-stream approach is described in detail in Verhoef and Bach (2003). According to this formulation, four terms are considered for describing the radiative transfer into the atmosphere in the VNIR and SWIR: i) the photons reflected by the atmosphere before reaching the surface, ii) the photons transmitted directly to the target and directly reflected to the sensor, iii) the photons that are scattered by the atmosphere before reaching the target and directly reflected to the sensor and finally iv) the photons that have at least two interactions with the atmosphere and one with the target. Taking these different contributions into account and considering the surface as uniform and Lambertian the Radiative Transfer Equations for the atmosphere can be written as:

$$E_s(b) = \tau_{ss}E_s(t) \tag{1}$$

$$E^-(b) = \tau_{sd}E_s(t) + \rho_{dd}E^+(b) \tag{2}$$

$$E_o(t) = \rho_{so}E_s(t) + \tau_{do}E^+(b) + \tau_{oo}E_o(b) \tag{3}$$

$$E^+(b) = \rho_{surf}[E_s(b) + E^-(b)] \tag{4}$$

where $E(b)$ and $E(t)$ indicate the bottom and the top of the atmosphere irradiance respectively, $E_s(b)$ is the direct solar flux, $E_0(t)$ is the top of atmosphere irradiance in the direction of viewing, $E^-(b)$ is the downward radiation from the sky, $E^+(b)$ is the diffuse upward flux, ρ_{so} is the bi-directional reflectance of the atmospheric layer, τ_{ss} is the down-welling direct transmittance, τ_{sd} is the diffuse transmittance in the solar direction, τ_{do} is the diffuse transmittance in the viewing direction, ρ_{dd} is the atmospheric spherical albedo, τ_{oo} is the up-welling direct transmittance and ρ_{surf} is the surface reflectance. Taking into account the Lambertian assumption for the surface, it implies that $E_o(b) = E^+(b)$, and using radiance units, $L_{TOA}(t) = E_o(t)/\pi$, the final RTE can be written as

$$L_{TOA} = \left(\rho_{so} + \frac{(\tau_{ss} + \tau_{sd})(\tau_{oo} + \tau_{do})}{1 - \rho_{surf}\rho_{dd}}\rho_{surf} \right) \frac{E_s}{\pi} \tag{5}$$

where L_{TOA} is the radiance measured at the top of the atmosphere that must be corrected atmospherically. E_s is the extraterrestrial solar irradiance. Using reflectance terms and by inversion of Eq. (5), we can finally obtain an expression for the surface reflectance ρ_{surf}:

$$\rho_{surf} = \frac{\rho_{TOA} - \rho_{so}}{(\tau_{do} + \tau_{oo})(\tau_{ss} + \tau_{sd}) + \rho_{dd}(\rho_{TOA} - \rho_{so})} \tag{6}$$

Application of Eq. (6) requires the computation of six atmospheric parameters τ_{do}, τ_{oo}, τ_{ss}, τ_{sd}, ρ_{dd} and ρ_{so}, which can be achieved from three MODTRAN4 runs for a uniform Lambertian surface reflectance

with spectrally flat surface albedos of 0, 0.5 and 1, as detailed in Verhoef and Bach (2003). Since test results were extracted for pixels located in flat and homogeneous areas, correction for adjacency effect was not considered in this paper. Details on this correction can be also found in Verhoef and Bach (2003).

2.2. Simplified approach based on MODTRAN calculations

MODTRAN4 follows the same formulation that the presented in the previous section, despite that notation is different for some terms. Among the direct outputs of MODTRAN4, one can find the TOA radiance and the extraterrestrial solar irradiance corrected for variations throughout the year in the earth-to-sun distance (i.e., solar irradiance is multiplied by the excentricity factor), labeled respectively as "TOTAL RAD" and "SOL@OBS". The earth-to-sun correction factor (sun elliptic orbit factor) and the solar zenithal angle (θ_z) are also given. Therefore, TOA reflectances can be easily computed according to:

$$\rho_{TOA} = \frac{\pi}{\cos\theta_z} \frac{(TOTAL\_RAD)}{(SOL@OBS)} \tag{7}$$

The proposed simplified approach is based on MODTRAN runs for different surface albedo values, in such a way that after computation of the corresponding ρ_{TOA} an empirical relationship $\rho_{surf} = f(\rho_{TOA})$ can be established. For example, in this paper 9 different MODTRAN runs have been considered, with surface albedo values from 0.l to 0.9 in steps of 0.1, and a second-order polynomial approach have been found to be accurate enough to relate ρ_{surf} with ρ_{TOA}:

$$\rho_{surf} = a\rho_{TOA}^2 + b\rho_{TOA} + c \tag{8}$$

Note that other MODTRAN runs could be considered, for example only from 0.1 to 0.7 (since is not very realistic to have surfaces with albedos >0.7), with a decreasing computing time, or even finest increments, which will increase the computing time. In all the cases presented in this paper, the statistical fit performed to obtain coefficients a, b and c in Eq. (8) provided correlation coefficients near to 1 (>0.999) and standard errors of estimation typically bellow 0.001 for VNIR and bellow 0.0001 for SWIR. For example, for the ASTER case discussed in Section 7.1, at-surface reflectance retrievals from this simplified approach and the one using the four-stream formulation (i.e., Eq. (8) versus Eq. (6)) differed in (-0.012 ± 0.002) for a bare soil plot and in (-0.009 ± 0.002) for a vegetated plot.

The simplified approach presented in this section does not account for surface elevation variations, neither for the adjacency effect. In this case more rigorous MODTRAN calculations in order to decouple all the involved parameters are required, similarly to the discussed in the four-stream formulation or as discussed in Guanter et al. (2009).

3. Theoretical basis for atmospheric correction in the TIR

Atmospheric correction in the TIR can be understood in two different ways: i) conversion of TOA radiance into radiance at ground-level (or land-leaving radiance) or ii) retrieval of Land Surface Temperature (LST) from the TOA radiance. As commented in the Introduction, strictly speaking, neither case (i) nor case (ii) can be considered a pure AC, since in case (i) the ground-level radiance still includes an atmospheric contribution due to the reflection term, and case (ii) includes also the correction of the emissivity, coupled to the atmospheric correction due again to the reflection term. Since the main objective when working with TIR data is the retrieval of the LST, we will focus our attention to case (ii). Similarly to the VNIR/SWIR case, we will consider a simplified approach to the direct inversion of RTE for LST retrieval from only one TIR band (case of Landsat5/TM). In the case of ASTER, with multispectral capabilities in the TIR region, we

will consider the Temperature and Emissivity Separation (TES) algorithm, explained bellow and which provides LST and also band emissivities. Note that in the case of only one TIR band emissivity should be estimated independently.

3.1. Radiative Transfer Equation

The Radiative Transfer Equation (RTE) applied to a particular wavelength (λ) in the TIR region and in its simplified form is given by

$$L_\lambda^{sen} = \left[\varepsilon_\lambda B_\lambda(T_s) + (1-\varepsilon_\lambda)L_\lambda^\downarrow\right]\tau_\lambda + L_\lambda^\uparrow \tag{9}$$

where L^{sen} is at-sensor registered radiance, B is the blackbody radiance, T_s is the LST, ε is the surface emissivity, τ is the atmospheric transmissivity, $L^\downarrow$ is the down-welling atmospheric irradiance normalized by π sr, and $L^\uparrow$ is the up-welling atmospheric path radiance. When applied to a certain sensor band, spectral magnitudes are averaged according to the spectral response function of that band. Eq. (9) is the starting point for many LST retrieval algorithms, as the ones described below. It is also possible to retrieve LST from direct inversion of RTE, i.e., extracting T_s from Eq. (9):

$$B_\lambda(T_s) = \frac{L_\lambda^{sen} - L_\lambda^\uparrow - \tau_\lambda(1-\varepsilon_\lambda)L_\lambda^\downarrow}{\tau_\lambda \varepsilon_\lambda} \tag{10}$$

T_s can be finally obtained by inverting Planck's law:

$$T_s = \frac{c_2}{\lambda}\left[\ln\left(\frac{c_1}{\lambda^5\left[\frac{L_\lambda^{sen}-L_\lambda^\uparrow}{\varepsilon_\lambda\tau_\lambda} - \left(\frac{1-\varepsilon_\lambda}{\varepsilon_\lambda}\right)L_\lambda^\downarrow\right]} + 1\right)\right]^{-1} \tag{11}$$

where the radiation constants are $c_1 = 1.19104 \times 10^8$ Wμm^{4}m^{-2}sr^{-1} and $c_2 = 14387.7$ μm K when λ is given in μm, radiance in W m^{-2}sr^{-1} μm^{-1} and temperature in K. Note that Eq. (11) requires the knowledge of atmospheric parameters τ, $L^\downarrow$, and $L^\uparrow$. Here-in-after spectral (or band) notation will be omitted for convenience.

3.2. Single-Channel algorithm for Landsat TM/ETM+

The Single-Channel (SC) algorithm is applied only to one TIR band, as is the case of TM or Enhanced TM+ sensors on-board the Landsat platforms. In particular, the SC$^{JM\&S}$ algorithm retrieves LST from one TIR band according to (Jiménez-Muñoz & Sobrino, 2003; Jiménez-Muñoz, 2009a):

$$T_s = \gamma\left[\frac{1}{\varepsilon}(\psi_1 L_{sen} + \psi_2) + \psi_3\right] + \delta \tag{12}$$

where γ and δ are two parameters dependent on the Planck's function and ψ_1, ψ_2 and ψ_3 are referred as Atmospheric Functions (AF) and given by:

$$\psi_1 = \frac{1}{\tau} \quad \psi_2 = -L^\downarrow - \frac{L^\uparrow}{\tau} \quad \psi_3 = L^\downarrow \tag{13}$$

Computation of AFs directly from Eq. (13) also requires the knowledge of atmospheric parameters τ, $L^\downarrow$, and $L^\uparrow$, although different approaches have been developed to retrieve AFs only from atmospheric water vapor content (Jiménez-Muñoz & Sobrino, 2003; Jiménez-Muñoz, 2009a) or water vapor and air temperature (Cristóbal et al., 2009). One of the main ideas behind the SC$^{JM\&S}$ algorithm was to provide an alternative to the direct inversion of RTE for retrieving LST, with Eq. (12) providing an easier formulation than the inversion one given by Eq. (11), and with AFs computed only from water vapor in order to avoid the dependence on atmospheric

parameters. Despite that Eq. (12) is an approximation to Eq. (11), when AFs are directly computed from Eq. (13) the SC$^{JM\&S}$ is nearly equivalent to apply direct inversion of RTE, thus providing similar accuracies on the LST retrieval. For example, in the Landsat5/TM case analyzed in Section 7.2, comparison between LST retrieved from SC algorithm and direct inversion of RTE provided a mean difference (bias) of (0.17 ± 0.06) K. When empirical approaches versus water vapor (or water vapor plus air temperature) are used for computing the AFs, some accuracy is lost at the expense of operationality. Again in the Landsat case, differences between LST retrieved from SC algorithm using approaches versus the water vapor content and the one retrieved from direct inversion of RTE provided a bias of (1.5 ± 0.2) K, as presented in Jiménez-Muñoz et al. (2009a).

3.3. Temperature and Emissivity Separation (TES) algorithm

Multispectral imaging capability of ASTER, with its five TIR channels, allows accurate retrieval of LST and LSE using the Temperature and Emissivity Separation (TES) algorithm (Gillespie et al., 1998). Basically, TES relies on an empirical relationship between spectral contrast and minimum emissivity, determined from laboratory and field emissivity spectra. This empirical relationship allows the equalization of the number of unknowns and measurements so that the set of Planck equations for the thermal radiances measured by ASTER can be inverted. Essentially, the empirical relationship is used to scale the emissivity spectra properly.

Inputs to TES algorithm are the atmospheric down-welling radiance, $L^{\downarrow}$, and the Land-Leaving Radiances (LLR), i.e., radiances at ground-level and therefore atmospherically corrected. From RTE the LLRs are given by:

$$LLR = \varepsilon B(T_s) + (1-\varepsilon)L^{\downarrow} \tag{14}$$

Therefore, from Eqs. (9) and (14), AC (case i discussed at the beginning of Section 3) reduces to:

$$LLR = \frac{L_{sen} - L^{\downarrow}}{\tau} \tag{15}$$

Note that application of TES algorithm also requires the knowledge of τ, $L^{\downarrow}$, and $L^{\uparrow}$.

4. Test area, field campaigns and imagery

Analysis of results and discussion will be focused on two particular cases in the framework of the SPECTRA Barrax Campaign (SPARC) and one particular case in the framework of the Sentinel-2 and Fluorescence Experiment (SEN2FLEX) field campaigns, carried out in July 2003 and July 2004 (SPARC) and in June/July 2005 (SEN2FLEX), and organized by European Space Agency (ESA) in the framework of its Earth Observation Envelope Programme (EOEP). Detailed information about the SPARC and SEN2FLEX campaigns can be found in Moreno et al. (2004) and at http://www.uv.es/~leo/sen2flex, respectively.

Both SPARC and SEN2FLEX field campaigns were carried out in the agricultural area of Barrax (39°3′ N, 2°6′ W, 700 m), located in the province of Albacete (Spain). The area has been selected in many other experiments due to its flat terrain, minimising the complications introduced by variable lighting geometry, and the presence of large and uniform land-use units, suitable for validating moderate-resolution satellite image products. The soils of the area are *Inceptisols* in terms of soil Taxonomy. About 65% of cultivated lands at Barrax are dryland (67% winter cereals; 33% fallow) and 35% irrigated land (75% corn; 15% barley/sunflower; 5% alfalfa; 5% onions and vegetables). More details about the test site are presented in Moreno et al. (2001).

Information about soil spectra and chemical composition can be found in Sobrino et al. (2009).

In the framework of the SPARC and SEN2FLEX campaigns, an intensive in-situ data collection was carried out, including among others radiometry, atmospheric characterization and vegetation parameters. Atmospheric profiles have been extracted for three particular dates: 23rd of July, 2003 (SPARC-2003), 18th of July, 2004 (SPARC-2004), and 13th of July 2005 (SEN2FLEX-2005). These three dates were selected for the optimal atmospheric conditions, the availability of local soundings, and the overpass of satellite imagery.

Satellite imagery used in this study included one CHRIS image acquired on 12th July, 2003, one ASTER image acquired on 18th July, 2004, and one Landsat5/TM image acquired on 13th July, 2005. These three images have been previously used in other works. See for example Guanter et al. (2005) and Jiménez-Muñoz et al. (2009b) for the CHRIS case, Sobrino et al. (2007) and Jiménez-Muñoz and Sobrino (2007, 2009) for the ASTER case, and Jiménez-Muñoz et al. (2009a) for the TM case.

CHRIS image was acquired in mode 1, with 62 spectral bands (covering the spectral range from 0.4 to 1.050 μm with a band-width of around 0.01 μm) and 34 m as spatial resolution. Since CHRIS instrument has multi-view capabilities, only the image acquired at near nadir view was considered in this paper. Note also that CHRIS has no TIR bands, so this image was employed only for at-surface reflectance retrievals. ASTER and TM sensor are well-known for the remote sensing community. Just as a reminder, ASTER has 3 VNIR bands (0.52–0.60; 0.63–0.69; 0.76–0.86 μm) at 15 m spatial resolution, 6 SWIR bands (1.6–1.7; 2.145–2.185; 2.185–225; 2.235–2.285; 2.295–2.365; 2.360–2.430 μm) at 30 m spatial resolution, and 5 TIR bands (8.125–8.475; 8.475–8.825; 8.925–9.275; 10.25–10.95; 10.95–11.65 μm) at 90 m spatial resolution. Landsat5/TM has 7 spectral bands, with bands 1, 2, 3, 4 in the VNIR (0.45–0.52; 0.52–0.60; 0.63–0.69; 0.76–0.90 μm), and bands 5 and 7 in the SWIR (1.55–1.75; 2.08–2.35 μm) at 30 m spatial resolution, and band 6 in the TIR (10.4–12.5 μm), at 120 m spatial resolution. Fig. 1 shows Spectral Response Functions (SRFs) of CHRIS, ASTER and TM bands over-plotted to an atmospheric transmissivity spectrum. As a reference, Fig. 2 shows a resize of the ASTER image for the test area of Barrax.

5. Atmospheric profiles

We provide in this section a description of the four different atmospheric profiles sources used in this study: i) local soundings (abbreviated as SOUND), ii) MODIS MOD07 product at 5 km spatial resolution, iii) Atmospheric Correction Parameter Calculator (ACPC) and iv) Modified Atmospheric Profiles from Reanalysis Information (MAPRI). Atmospheric profiles extracted from the different sources were converted to MODTRAN4 format in order to compute the different variables, ρ_{TOA} in the case of VNIR–SWIR and atmospheric parameters τ, $L^{\downarrow}$, and $L^{\uparrow}$ in the case of TIR. Spectral outputs were averaged using the SRFs of the sensors. MODTRAN4 was executed in every case with multiple scattering using 16-streams in the Discrete Ordinates Radiative Transfer Program for a Multi-Layered Plane-Parallel Medium (DISORT) algorithm (Stamnes et al., 1988). Minor atmospheric constituents were assigned to the mid-latitude summer standard atmosphere included in MODTRAN, assumed to be representative of atmospheric conditions in June and July in Spain. It is worth to mention that MODTRAN provides as an output the parameter $L^{\downarrow}$ for a given observation angle. A complete calculation of the reflection term requires the evaluation of $L^{\downarrow}$ at all view angles covering the hemisphere. In this paper we have used only the $L^{\downarrow}$ value at nadir instead of the hemispheric one. This approach avoids computation of MODTRAN at different view angles (thus saving computing time), and errors on the final LST retrieval due to this assumption are minimal for high emissivities, as is the case of the agricultural area considered in this study.

(a)

(b)

(c)

(d)
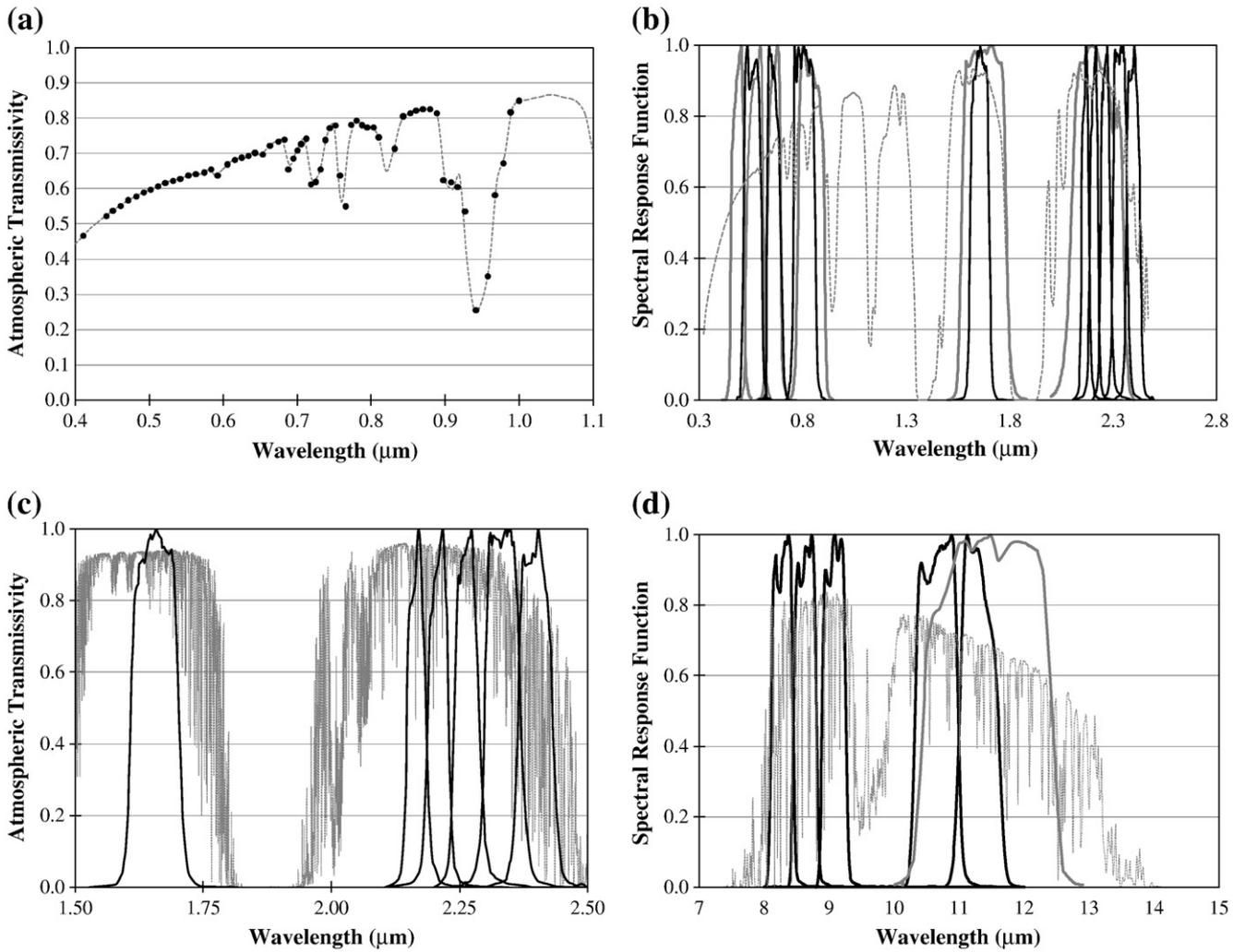
Fig. 1. Spectral response functions for the bands of sensors considered in this study. (a) CHRIS bands overlapped to a smoothed transmisivity spectrum. (b) ASTER and Landsat5/TM VNIR and SWIR bands overlapped to a smoothed transmissivity spectrum. (c) ASTER SWIR bands overlapped to a fine spectral resolution (1 cm^{-1}) transmissivity spectrum. (d) ASTER and Landsat5/TM TIR bands overlapped to a fine spectral resolution (1 cm^{-1}) transmissivity spectrum.
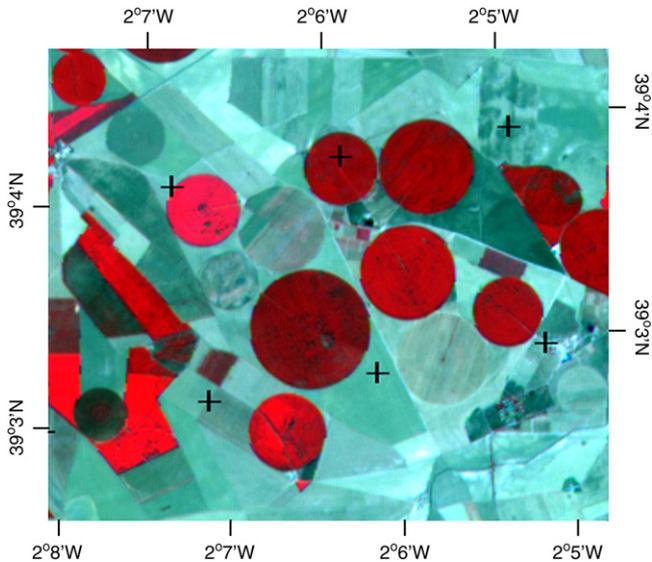
Fig. 2. Index map for the Barrax test area extracted from a RGB composition using ASTER VNIR bands 3, 2 and 1 (18 July 2004).

Conversion to appropriate data format and execution of MOD-TRAN4 required further processing of MOD07, as it is explained bellow. Processing of SOUND and ACPC profiles was minimal, since they were provided almost in the appropriate format. On the other hand, it should be noted that MAPRI provides an improvement to other existing Reanalysis-based profiles, since data at 17 levels were interpolated to 34 levels, and the original spatial resolution of $2.5° \times 2.5°$ was regrided to $0.5° \times 0.5°$, as will be explained also bellow.

5.1. Local soundings

In the framework of the SPARC and SEN2FLEX field campaigns daily local soundings were launched near the overpass time of different airborne and satellite sensors. Vertical structure of the atmosphere was characterized from Vaisala RS80 radiosondes, which are small sensors integrated in a light box and released into the atmosphere on meteorological helium filled balloons. Pressure, temperature and humidity are measured at regular intervals and transmitted to the surface by radio signals. The equipment was completed with a ground station AIR Inc. TS-2AR Receiver s/n 259 for the signal reception. The altitude of the sonde was computed using the hydrostatic equation, which is a function of the pressure. Relative humidity is directly measured by a capacitive thin film sensor with

reliable response even at low temperatures and after exposure to condensation. Wind speed and direction are not directly measured but computed by the ground equipment from the GPS information about the sonde position.

For the 12th July 2003 test case, the radiosounding was launched at 11:11 UTC, and it reached a final altitude of around 26 km at 12:39 UTC. For the 18th July 2004 test case, it was launched at 10:13 UTC and it reached a final altitude of around 27 km at 11:41 UTC. For the 13th July 2005 test case, it was launched at 10:48 UTC, it reached a final altitude of around 24 km, ending at around 12:07 UTC. Additional information of radiosoundings and atmosphere characterization can be found in Molero et al. (2005) and Molero et al. (2006).

5.2. MODIS atmospheric profiles product (MOD07)

The MODIS project provides the scientific community with many Standard Products, the atmospheric profiles product among them, denoted as MOD07 or MYD07 when the Terra or Aqua platform is used, respectively. In general, we will use the term MOD07 to refer both Terra and Aqua derived products.

MOD07 consists of several parameters, such as total-ozone burden, atmospheric stability, temperature and moisture profiles, and atmospheric water vapor. All of these parameters are produced day and night at 5×5 1-km pixel resolution when at least 9 observations are cloud free. It provides a total amount of 20 atmospheric levels. In particular, the pressure levels of profiles are 5, 10, 20, 30, 50, 70, 100, 150, 200, 250, 300, 400, 500, 620, 700, 780, 850, 920, 950 and 1000 hPa.

MOD07 product is generated from an algorithm for retrieving vertical profiles of atmospheric temperature and moisture from multi-wavelength thermal radiation measurements in clear skies. While MODIS is not a sounding instrument, it does have many of the spectral bands found in other sounding instruments, so it is possible to generate profiles of temperature and moisture as well as total column estimates of precipitable water vapor, ozone, and atmospheric stability from its infrared radiance measurements. Basically, the algorithm is a statistical regression with the option for a subsequent non-linear physical retrieval. It is not the scope of this paper to focus on the algorithm retrieval. The reader can find a detailed description in the Algorithm Theoretical Basis Documents (ATBD) (Seemann et al. 2006) and MODIS Atmosphere Web site at http://modis-atmos.gsfc.nasa.gov/.

MOD07 products were downloaded from the MODIS web page for the desired dates (12th July 2003, at 11:25 UTC, 18th July 2004, at 11:00 UTC, and 13th July 2005, at 11:45 UTC) in Hierarchical Data Format (HDF), which includes the atmospheric data at 5×5 1-km pixel resolution plus ancillary data such as the latitude and longitude. For a given pixel, i.e., for a given latitude and longitude, values of air temperature, dew point temperature and geopotential height were extracted from MOD07 for the 20 nominal pressure levels.

MOD07 profiles were extracted for one single pixel centered at Barrax latitude and longitude, but also for the whole Iberian Peninsula in order to generate maps of atmospheric parameters in the case of TIR and observe their spatial distribution. In this last case it should be noted that the computing time using normal computers is excessive, around 100 h for the test cases presented in this study. The problem of computing time could be solved by using other processing techniques, such as parallel processing and faster machines, but it is not within the scope of this paper. Computing time could be also saved by changing some MODTRAN execution parameters, such as increasing the spectral interval and/or decreasing the number of streams in the DISORT algorithm.

Fig. 3 shows a reference index map of MOD07 products for SPARC-2004 and SEN2FLEX-2005 test cases over the Iberian Peninsula. Fig. 4 shows the TIR atmospheric parameters maps obtained from MOD07 and MODTRAN executions for the ASTER case (18 July 2004), and Fig. 5 shows the maps obtained for the Landsat5/TM case (13 July 2005). In this last case maps of AFs (see Section 3.2, Eq. (13)) are also provided.

5.3. Atmospheric profiles from Atmospheric Correction Parameter Calculation (ACPC)

An Atmospheric Correction Parameter Calculation (ACPC) web-tool was proposed by Barsi et al. (2003; 2005) in order to provide atmospheric parameters particularized to the Landsat5/TM and Landsat7/ETM + TIR bands. In addition to these parameters, the vertical profile is also provided to the user.

Data included in the ACPC is generated by the National Center for Environmental Prediction (NCEP), and they incorporate satellite and surface data to predict a global atmosphere at 28 altitudes, plus one extra altitude at the TOA (at 0 hPa). These modelled profiles are sampled on a $1° \times 1°$ grid and generated every 6 h, 00:00, 06:00, 12:00, and 18:00 UTC. Vertical atmospheric information includes the most important variables such as pressure, geopotential height, air temperature and relative humidity, among others. Despite that ACPC is a very useful tool for AC of Landsat data, at this moment information is only available from 1st March 2000 to present. In addition, in the web-based tool the user needs to introduce the latitude and longitude coordinates for one single case, and results are sent by e-mail, which jeopardizes its operational use.

5.4. Modified Atmospheric Profiles from Reanalysis Information (MAPRI)

Other sources of atmospheric profiles rely on the dataset provided by NCEP and the National Center of Atmospheric Research (NCAR) Reanalysis project (NCEP-1 here-in-after). NCEP-1 is a completely free available meteorological and climatological database often used for weather forecast and climate assessments. It covers a time period of about 60 years (from 1948 to nowadays), and it includes several meteorological variables at surface and 17 mandatory atmospheric levels, among others (Kistler et al., 2001).

In this study, relative humidity, air temperature and geopotential height variables have been extracted from daily data given by the NCEP-1 for 12th July 2003, 18th July 2004 and 13th July 2005, all three at 12 UTC. That dataset follows the atmospheric mandatory levels at 1000, 925, 850, 700, 600, 500, 400, 300 hPa in the case of relative humidity and additionally 250, 200, 150, 100, 70, 50, 30, 20, 10 hPa for air temperature and geopotential height. The spatial resolution is $2.5° \times 2.5°$ latitude–longitude in a global grid (Kalnay et al., 1996). Reanalysis data was downloaded in a global scale as .nc format and processed with Interactive Data Language (IDL) covering an area from 35° to 45° N, and from 10° W to 5° E. Finally, resulting images were saved as binary format.

Binary images were interpolated in order to improve the spatial and vertical resolution. First, images of atmospheric variables (height, temperature and humidity) were resampled applying a bilinear method to convert the spatial resolutions of 2.5° to 0.5°. Such interpolation was performed for each mandatory level. In this context, there are other works which applied a linear or quadratic interpolation method over Reanalysis data type for comparing with other datasets used for global change or climate studies (Delbart et al., 2008; Ngo-Duc et al., 2005; Sobrino et al., 2006). Once the spatial resolution was improved, the original vertical resolution with 17 mandatory levels was converted to 34 levels, using for this purpose a cubic spline segment interpolation method. Note that in the case of relative humidity, with only 8 mandatory levels, the interpolation provided 16 levels, so for the rest of levels values from the mid-latitude summer standard atmosphere included in MODTRAN was considered. The spline interpolation used a vector of points $[x_i, y_i]$ $(i = 0, 1, ..., n)$, with a piecewise continuous curve passing through each of the values following Eq. (16):

$$S_i(x) = a_i(x-x_i)^3 + b_i(x-x_i)^2 + c_i(x-x_i) + d_i \quad x \in [x_i, x_{i+1}] \quad (16)$$

where a_i, b_i, c_i and d_i are the coefficients and $S(x)$ is the cubic spline interpolation. Absolute accuracy of this interpolation method has not been assessed yet, but this issue will be addressed in a future work
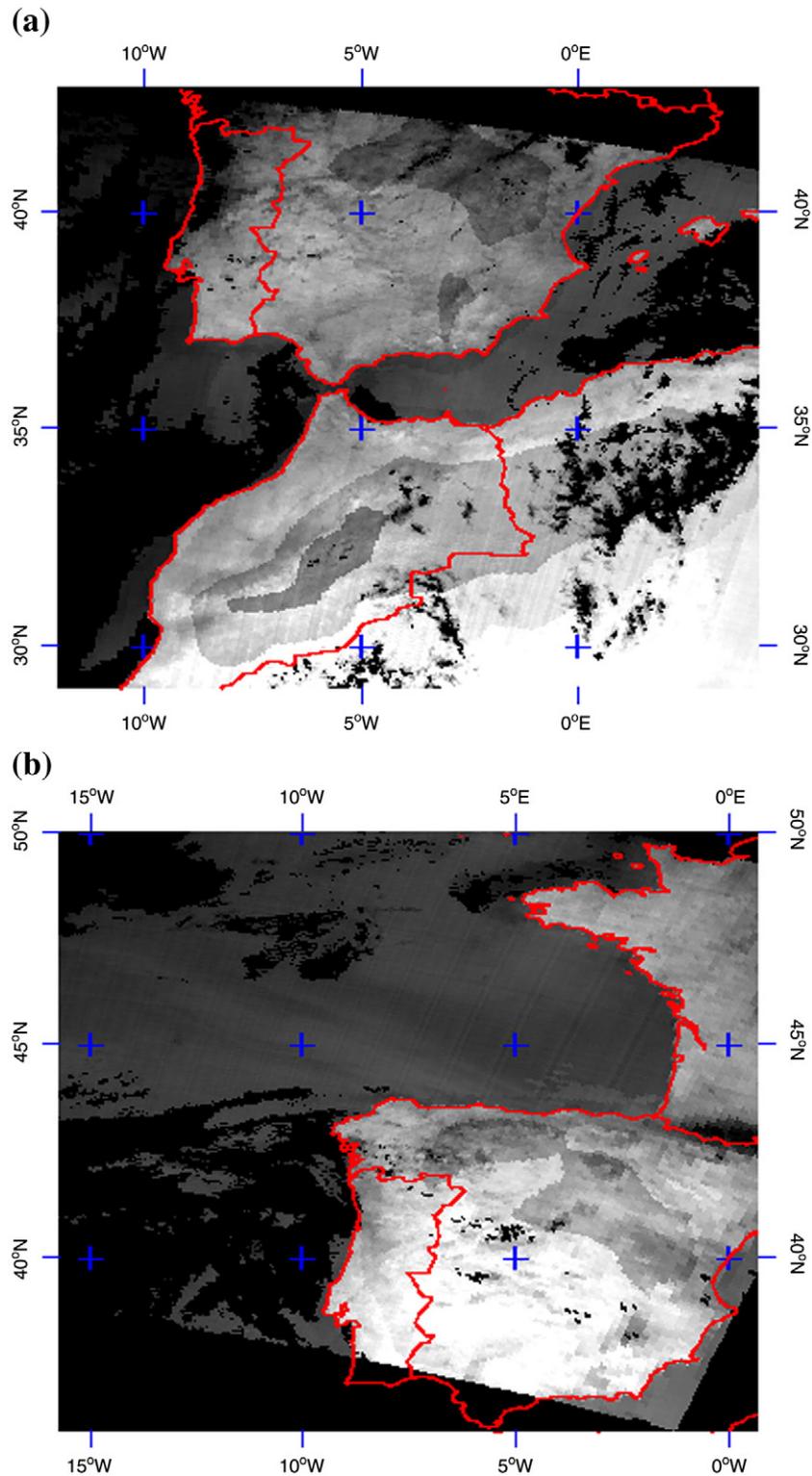
Fig. 3. Index maps of temperature at first atmospheric level for the Iberian Peninsula extracted from MOD07 products. a) Image acquired on 18th July 2004, scaled from 290 K (black) to 316 K (white). b) Image acquired on 13th July 2005, scaled from 289 K (black) to 309 K (white).

describing in detail a MAPRI database constructed over Europe. Appropriate performance of the proposed methodology is demonstrated by the results presented in Sections 6 and 7.

6. Intercomparison of vertical profiles

Vertical structures for the four atmospheric profiles (SOUND, MOD07, ACPC and MAPRI) at the three different dates (12th July 2003,

18th July 2004 and 13th July 2005) were intercompared to analyze differences between them. The implication of these differences in the atmospheric correction is analyzed in the next section.

Air and dew point temperatures at different pressure levels are plotted in Fig. 6 for the different profiles sources and dates. MOD07, ACPC and MAPRI provide similar air temperature profiles than SOUND, in particular for pressure levels between 600 and 200 hPa. The highest differences are observed for MOD07 at lowest altitude
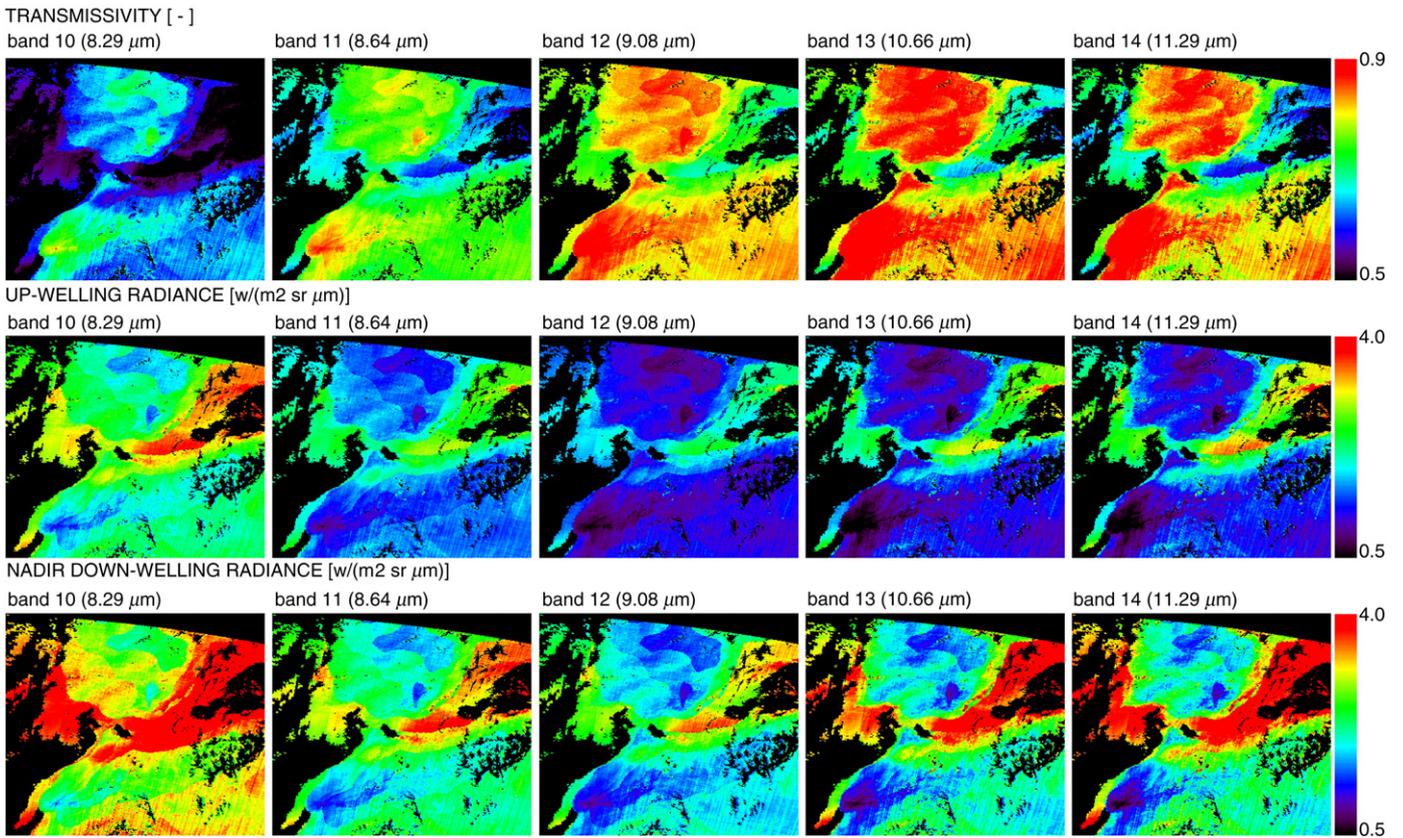
Fig. 4. Atmospheric parameters maps over the Iberian Peninsula for ASTER TIR bands generated from MOD07 product (acquired on 18th July 2004) and MODTRAN4 radiative transfer code. See index map in Fig. 3a.

levels (approximately between 1000 and 800 hPa), specially for the 2004 and 2005 test cases, with differences >6 K, and for MAPRI at the 100 hPa level, with differences >7 K. ACPC provides the best agreement with SOUND, but significant differences are found at the first level (near 1000 hPa) in 2004 and 2005 cases, with differences >10 K. An anomalous tendency is also observed at the highest altitude levels of ACPC (near to 0 hPa), with an extreme decrease on air temperature, reaching the value of 190 K in the three cases. This is due to the addition of the extra level in the ACPC profiles.

Differences notably higher were found in the dew point temperature profiles. Despite that a similar behavior is observed at lowest levels (approximately between 1000 and 700 hPa) and those levels approximately between 400 and 100 hPa (except for the 2003 test case, when differences are slightly higher), huge differences are observed at the region between 700 and 400 hPa. In this region a significant decrease on the dew point temperature was observed by SOUND. ACPC was sensitive to this decrease, but MOD07 and MAPRI did not registered that abrupt change, although in 2004 MAPRI seems
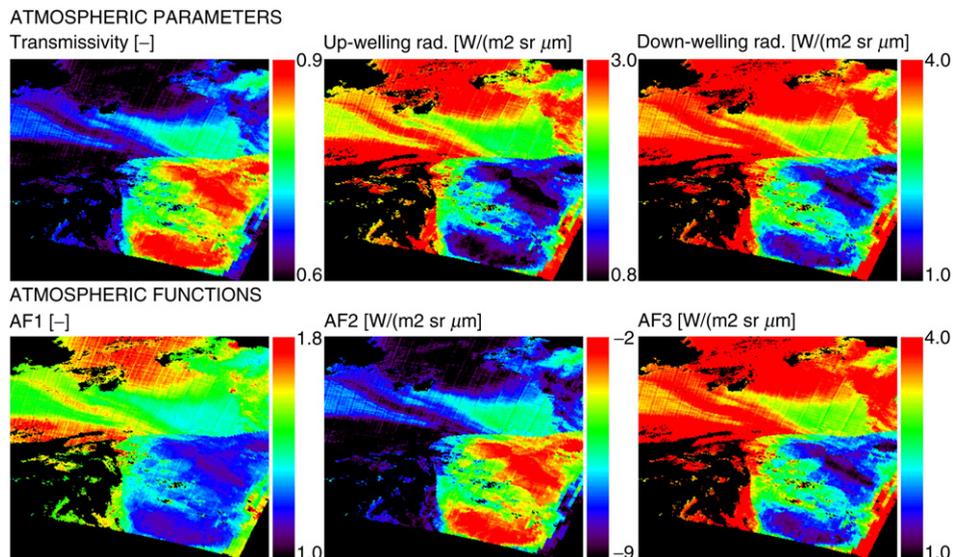
Fig. 5. Atmospheric parameters and functions maps over the Iberian Peninsula for Landsat5/TM TIR band 6 generated from MOD07 product (acquired on 13th July 2005) and MODTRAN4 radiative transfer code. See index map in Fig. 3b.
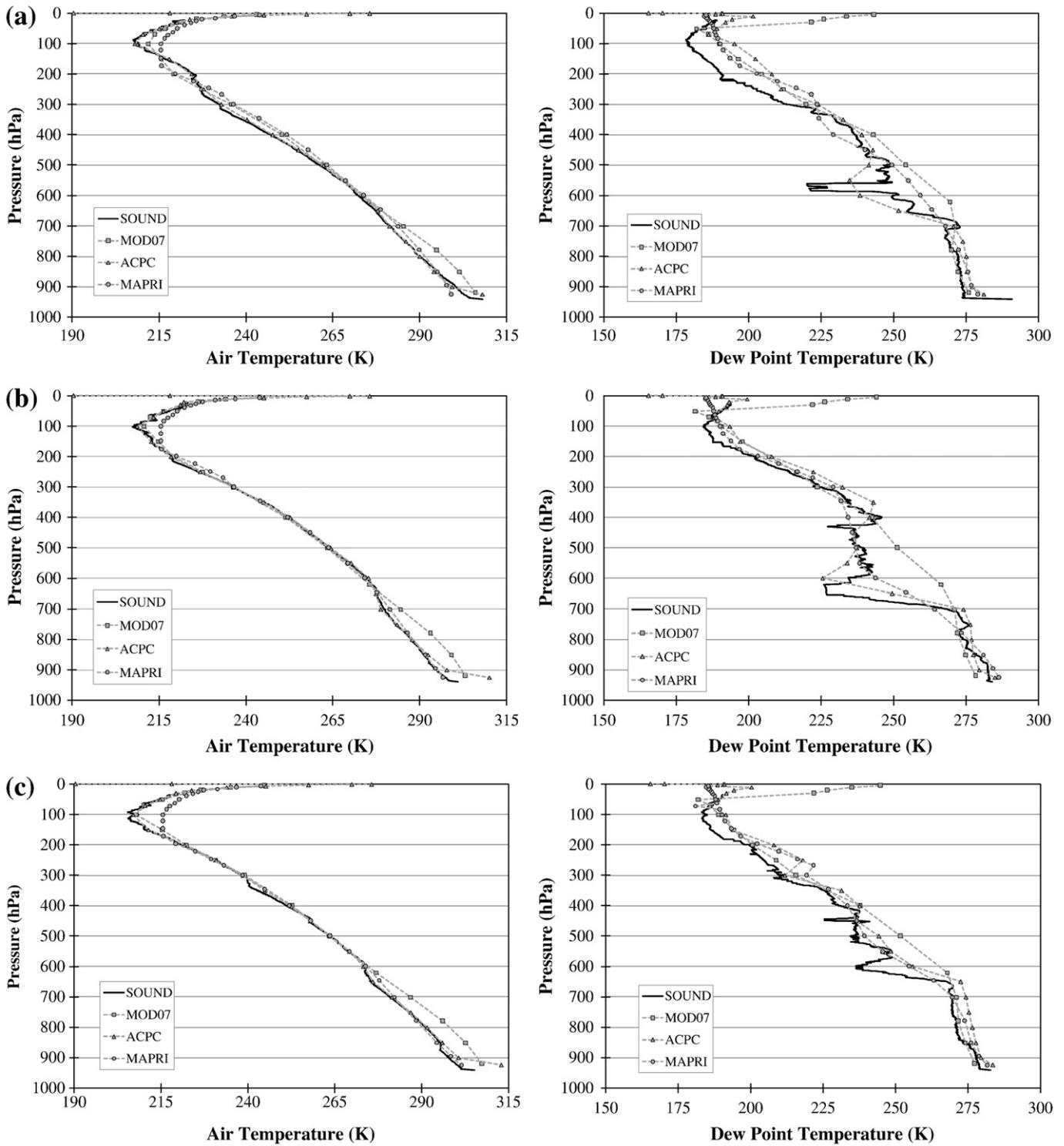
Fig. 6. Vertical distribution of air (left column) and dew point (right column) temperatures extracted from the four different atmospheric profiles sources on a) 12th July 2003, b) 18th July 2004 and c) 13th July 2005.

to detect slightly that feature. This effect could be attributed to a scale problem, in which a local atmospheric phenomenon can be observed by a local sounding but not by the other profiles, averaged at 5-km in the case of MOD07, at 50-km in the case of MAPRI and around 100-km in the case of ACPC. An extremely high difference was observed in the case of the MOD07 product at the highest altitude levels (<100 hPa), with differences >25 K, which could be due to a failure in the MOD07 algorithm retrieval at levels near the TOA, characterized by very low

humidity and water vapor content. Again, the anomalous tendency was observed for ACPC at the TOA (near 0 hPa).

Integration of water density content over altitude allows the retrieval of the total atmospheric water vapor content for a given profile, which is a key atmospheric variable in the AC. Table 1 shows the values obtained from the different profiles for the different dates. In 2003 and 2004 test cases, SOUND, ACPC and MAPRI provided similar values, between 1.5 and 1.7 g/cm^2, whereas MOD07 overestimated

Table 1
Total atmospheric water vapor content (in g/cm^2) retrieved from the four atmospheric profiles at the three different dates used as a test case.

	12Jul03	18Jul04	13Jul05
SOUND	1.62	1.74	1.58
MOD07	2.11	2.14	2.12
ACPC	1.54	1.71	1.93
MAPRI	1.69	1.74	2.37

slightly this quantity (2.1 g/cm^2). In 2005, all the four profiles provided slightly different results, 1.6, 2.1, 1.9 and 2.4 for SOUND, MOD07, ACPC and MAPRI, respectively.

7. Atmospheric correction results

In the previous section differences on the vertical profiles were analyzed to observe the consistency between the different products. However, it is not the objective of the paper to analyze those differences in an atmospheric science perspective. Since we are only interested on what those differences imply in terms of the atmospheric correction, i.e., differences in the retrieval of surface reflectances and land surface temperature (and also emissivity in the case of ASTER), we show in this section the results obtained in the AC of the different band sensors using the four atmospheric profiles databases.

7.1. VNIR and SWIR spectral ranges

In the case of AC in the VNIR and SWIR regions, the AOT content at 550 nm is required additionally to the atmospheric profile. As far as we know, there is no Reanalysis-based information about this variable, so values were extracted from MODIS aerosol product (MOD04) and also retrieved from ground-based measurements using a CIMEL CE318-NE Sun photometer, as explained for example in Estellés et al. (2008). Values are provided in Table 2. Note that MOD04 values are around AOT = 0.3, whereas field-based ones are around 0.2. It has been previously reported the problem of AOT overestimation at low AOT values for the MOD04 product (Levy et al., 2005), especially for version 4 compared to version 5 (Papadimas et al., 2008), despite some attempts are proposed to correct the bias (Lary et al., 2009). Therefore, we considered AOTs of 0.1, 0.2 and 0.3 in the retrievals to assess the impact of this uncertainty.

In addition to the intercomparison of at-surface reflectance retrievals from the different vertical profiles, these retrievals are also compared to ground-based measurements using an Analytical Spectral Devices (ASD) FieldSpect Pro FR Spectroradiometer, which covers the spectral range between 0.35 and 2.5 μm with a spectral resolution of 0.001 μm. Test plots selected were vegetation (alfalfa) and bare soil. Additionally, CHRIS retrievals were compared to the ones provided by the BEAM software (http://www.brockmann-consult.de/cms/web/beam), an open-source toolbox and development platform for viewing, analysing and processing of remote sensing raster data, which includes, among others, the AC of CHRIS data following the procedure described in

Table 2
Aerosol Optical Thickness at 550 nm extracted from MODIS product (MOD04) and in-situ measurements with a CIMEL Sun photometer for the three different dates used as test cases. Standard deviation for the mean value of central pixel and its neighborhood pixels is provided in the case of MOD04, and standard deviation for a time window centered at 11:00 UTC is provided in the case of CIMEL measurements (they are given in brackets). AOT for MOD04 on 18th July 2004 was extracted only for one pixel (rest of pixels provided invalid values), so standard deviation is not available.

	12Jul03	18Jul04	13Jul05
MOD04	0.26 (0.06)	0.30 (N/A)	0.28 (0.05)
CIMEL	0.17 (0.02)	0.21 (0.03)	0.24 (0.05)

Guanter et al. (2005), whereas ASTER retrievals were also compared to the Standard Product AST07.

7.1.1. CHRIS (12 July 2003)

Previously to the analysis of results retrieved from CHRIS data, it is worth to mention that this sensor has some miscalibration problems due to its "technology demonstrator" nature. As a result, the retrieved reflectance spectrum shows anomalous variations or unexpected peaks, especially at lowest (near to 0.4 μm) and highest (>700 μm) wavelengths. It is not the scope of this paper to address these issues, but to compare differences on the spectrum due to the use of different atmospheric profiles. A dedicated atmospheric correction algorithm which includes retrieval of coefficients for solving the calibration problem was presented in Guanter et al. (2005). This solution is also implemented in the BEAM software, denoted as "spectral polishing".

Fig. 7 shows surface reflectance retrievals over vegetation and bare soil using the SOUND profile for AOT values of 0.1, 0.2 and 0.3 (Fig. 7a), the different atmospheric profiles (Fig. 7b) and the BEAM processor in the AC (Fig. 7c). In-situ reflectance values measured with the ASD instrument are also plotted in all cases. If we focus on retrievals over alfalfa plot for different AOTs (Fig. 7a, left), we can observe that AOT = 0.2 is the case which better fits with the in-situ measurement, which agrees also with the AOT value measured in-situ (see Table 2). An AOT value of 0.3 underestimates the surface reflectance in the visible region (approximately between 0.4 and 0.7 μm), whereas when using an AOT of 0.1 it is overestimated. Around the red edge region reflectance retrievals agree with in-situ measurements almost independently of the AOT value considered. Far from this region, retrievals are also quite similar for the three AOT values considered, but they depart significantly from the in-situ measurement. This corroborates something well-known when working in AC of optical imagery, and is that AOT uncertainty affects mainly to the visible region and not to the near-infrared one. This result is also evident in the bare soil plot (Fig. 7a, right), but note that in this case an AOT = 0.3 seems to fit better with the in-situ measurement. It should be taken into account that directional effects are higher in bare surfaces than fully-vegetated ones (as is the case of the alfalfa plot), and CHRIS acquisition was not totally at a nadir view, but at around 28° instead. For this reason, we will use as reference the alfalfa plot and consider an AOT value of 0.2 as the "truth", which was coincident with the in-situ measurement and also with the value extracted automatically from the image according to Guanter et al. (2005).

Intercomparison of surface reflectances obtained using the different atmospheric profiles (with an AOT value fixed at 0.2) is provided in Fig. 7b for the alfalfa and bare soil plots. They show that surface reflectance retrievals in the visible region are almost insensitive to the atmospheric profile used, and only appreciable differences are observed at near-infrared bands, especially in the region between 0.9 and 1 μm where a strong absorption band due to water vapor is located. Since different atmospheric profiles provide different water vapor contents, differences are due to variations on this variable. In the visible region (and red edge) differences due to water vapor contents are not observed, since in this region the main contribution to the AC is the AOT, as stated before.

In comparison to the retrievals provided by the BEAM AC, the ones retrieved using the SOUND profile agreed better with in-situ measurements in the case of the alfalfa plot (Fig. 7c, left), but BEAM AC provided better results in the case of bare soil (Fig. 7c, right). In any case, retrievals from BEAM and the methodology used in this paper are quite similar. Note that the "spectral polishing" option included in BEAM provides a smooth spectrum, in better accordance with field measurements since strange peaks are removed.

7.1.2. ASTER (18 July 2004)

Reflectance retrievals from ASTER VNIR and SWIR bands are presented in Fig. 8. In particular, Fig. 8a shows differences on the
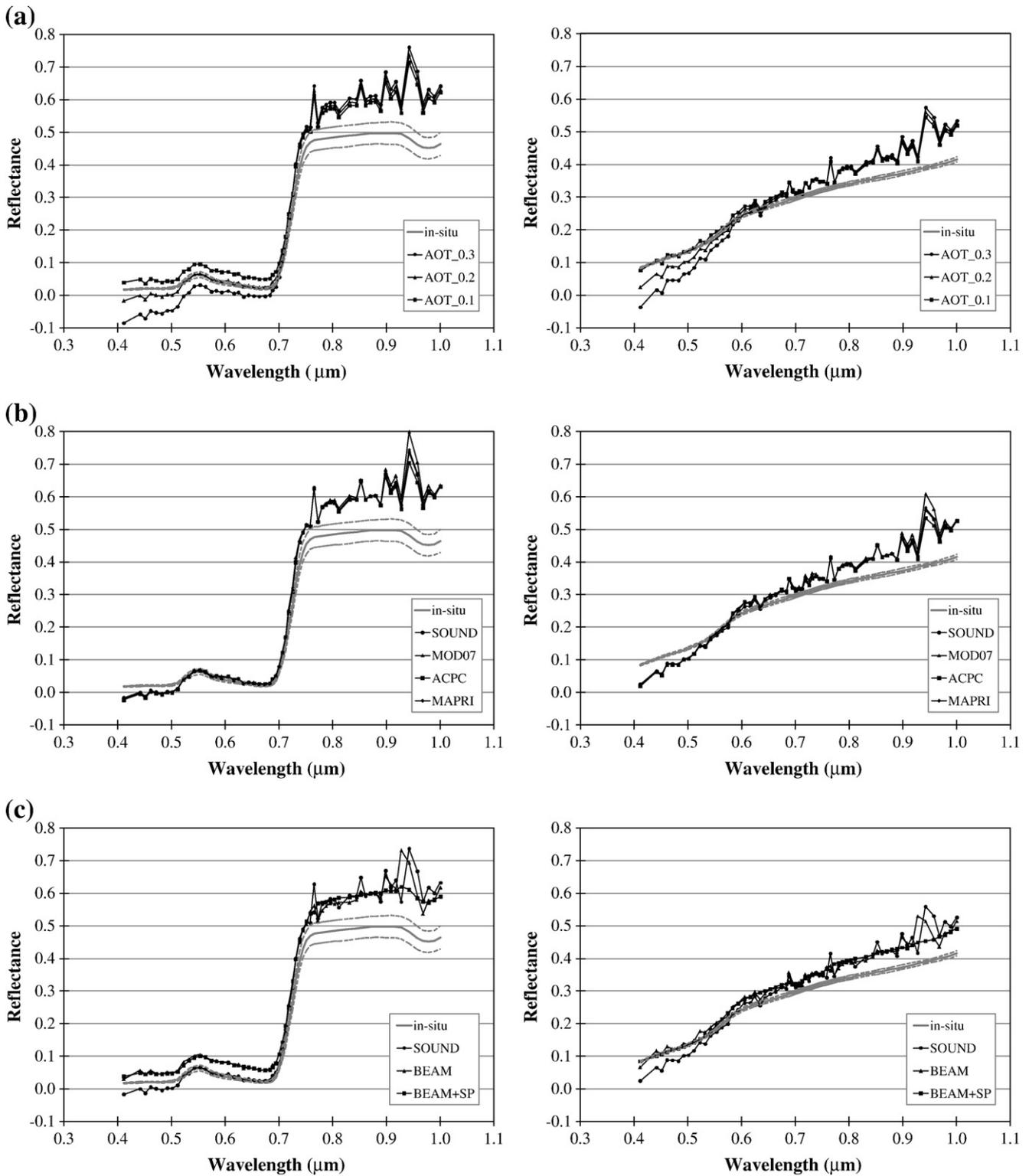
Fig. 7. Surface reflectance retrievals from CHRIS data acquired on 12th July 2003 over alfalfa (left column) and bare soil (right column). (a) Comparison between retrievals using local sounding for atmospheric correction and different Aerosol Optical Thickness (AOT) at 550 nm values (0.1, 0.2 and 0.3) and the spectrum measured in-situ. (b) Comparison between retrievals using the different atmospheric profiles for an AOT content fixed at 0.2 and the spectrum measured in-situ. (c) Comparison between retrievals using local sounding for atmospheric correction and the ones provided by the BEAM software, assuming an AOT of 0.2.

reflectance spectrum due to different AOT using the SOUND atmospheric profile for green grass and bare soil plots. In the case of green grass plot, it was cut at the moment of the retrieval, so the spectrum is slightly different to fully-covered vegetation like the alfalfa plot used in the CHRIS analysis. Note also that ASTER has not a blue band, which is the most sensitive to AOT. According to results

obtained for bands 1 and 2 (located in the green and red regions) in the green grass plot (Fig. 8a, left), it seems that an AOT content of 0.1 fits better with the in-situ measurements, and an AOT of 0.3 clearly underestimates the reflectance. Rest of bands are almost insensitive to AOT content. Retrievals depending on the atmospheric profile used are presented in Fig. 8b for green grass and bare soil, in which an
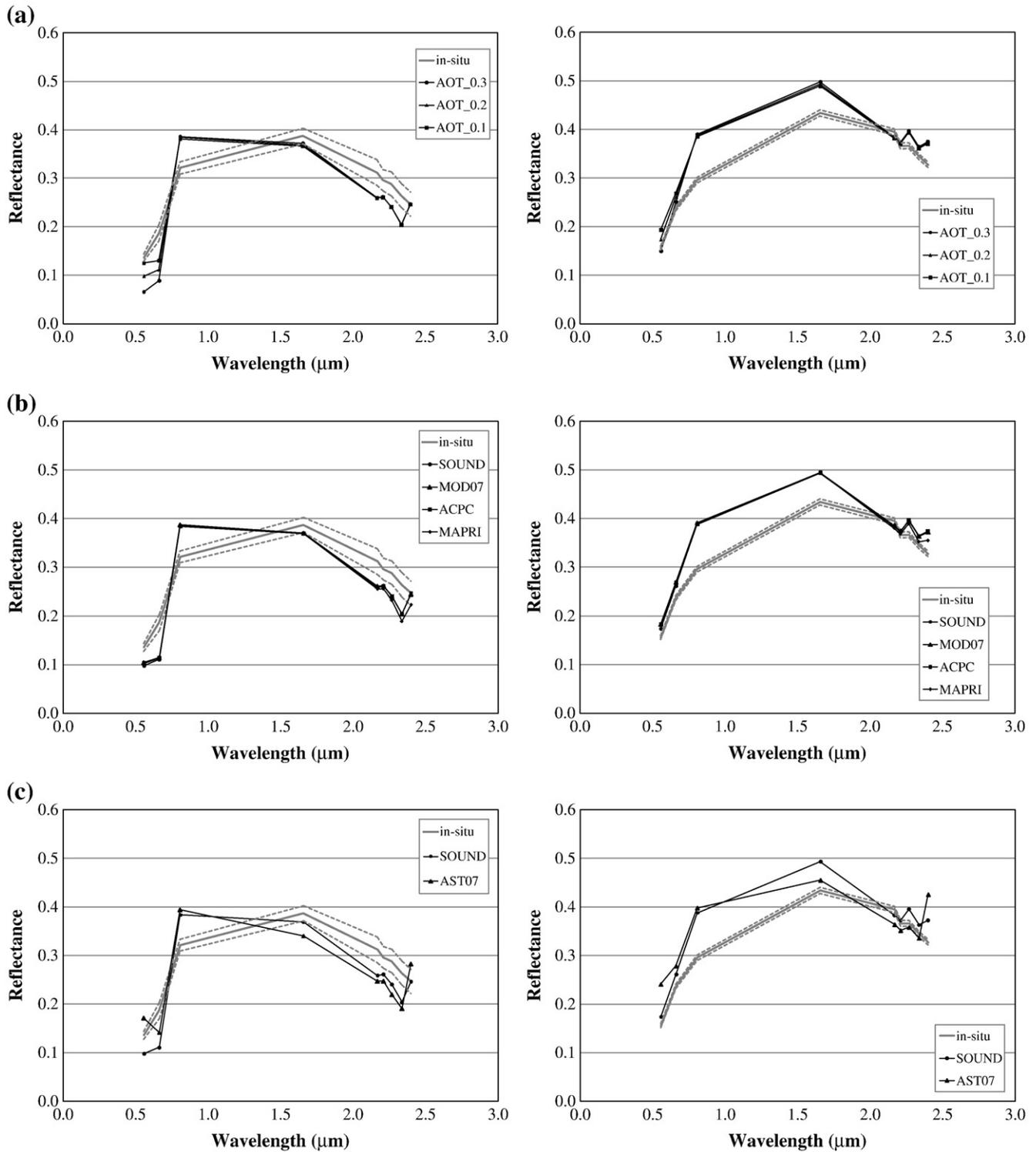
Fig. 8. Surface reflectance retrievals from ASTER data acquired on 18th July 2004 over green grass recently cut (left column) and bare soil (right column). (a) Comparison between retrievals using local sounding for atmospheric correction and different Aerosol Optical Thickness (AOT) at 550 nm values (0.1, 0.2 and 0.3) and the spectrum measured in-situ. (b) Comparison between retrievals using the different atmospheric profiles for an AOT content fixed at 0.2 and the spectrum measured in-situ. (c) Comparison between retrievals using local sounding for atmospheric correction and an AOT of 0.2, and the ones provided by the ASTER Standard Product AST07.

AOT = 0.2 has been considered, since it is the value measured in-situ despite that according to Fig. 8a a value of 0.1 fits better with in-situ measurements. Significant differences were not found when using the different atmospheric profiles. Only small differences were observed at SWIR bands between 2 and 2.5 μm, which are located in regions affected by water vapor absorption features (see Fig. 1). In Fig. 8c

reflectance extracted from the ASTER standard product (AST07) was compared to the one retrieved using SOUND (with AOT = 0.2) and the methodology proposed in this paper (i.e., statistical fit between ρ_{surf} and ρ_{TOA} using MODTRAN4 computations). This last retrieval improves AST07 results at bands 1 (0.56 μm) and 9 (2.4 μm). At the rest of bands differences between AST07 and SOUND are smaller.

Hence, when compared to the in-situ measurement, a Root Mean Square Error (RMSE) of 0.06 for AST07 and 0.04 for SOUND was obtained.

7.1.3. TM (13 July 2005)

Reflectance spectra obtained for TM VNIR and SWIR bands over festuca and bare soil plots are presented in Fig. 9. Results are similar to the ones analyzed in the ASTER case, i.e., an AOT content of 0.1 seems to fit better with in-situ measurements, despite that the value measured in-situ was 0.2. The value of 0.3 provided by MOD04 underestimates the reflectance. NIR and SWIR bands are almost insensitive to the AOT content, and also to the water vapor content (as it is observed in the intercomparison of different atmospheric profiles). Note that in the case of ASTER, a light sensitivity was observed in the case of SWIR bands. The different behavior between ASTER and TM SWIR bands is explained because of the wider bandwidth of the TM sensor compared to the ASTER one (see Fig. 1 for bands configuration).

7.2. TIR spectral range

Analysis of results on the TIR region was focussed on ASTER and TM instruments, since CHRIS does not have TIR bands. In the case of ASTER, both LST and surface emissivities were retrieved with the TES algorithm using the different atmospheric profiles as input in the AC.

In the case of TM, only LST was retrieved (since it only has one TIR band) with the Single-Channel algorithm, and emissivity was computed from the NDVI approach as explained in Jiménez-Muñoz et al. (2009a). Despite that a complete dataset of thermal measurements was collected in the framework of SPARC and SEN2FLEX campaigns, they were focussed on the calibration/validation of airborne data at very high spatial resolution (between 2 and 6 meters). Part of the measurements was useful for validation of ASTER retrievals at 90 m spatial resolution, as presented in Sobrino et al. (2007). However, measurements were not suitable for the TM case, at 120 m spatial resolution. For this reason, and in order to have a strong statistic, we considered as a ground-truth the LST image (or emissivity images) retrieved from the SOUND profile, in such a way that LST retrievals from the other profiles were compared to the SOUND one in a pixel per pixel basis. Focussing only on the test site, the resized image over that area provided more than 2000 pixels to extract statistics.

7.2.1. ASTER (18 July 2004)

Previously to the comparison of LST retrievals, we compared the atmospheric parameters involved in the AC for the five ASTER TIR bands. Results are graphed in Fig. 10. MOD07 provided the worst agreement with SOUND data, with differences being higher with increasing wavelength, something *a priori* unexpected since bands 13 (10.7 μm) and 14 (11.3 μm) are less affected by atmospheric absorption. ACPC and
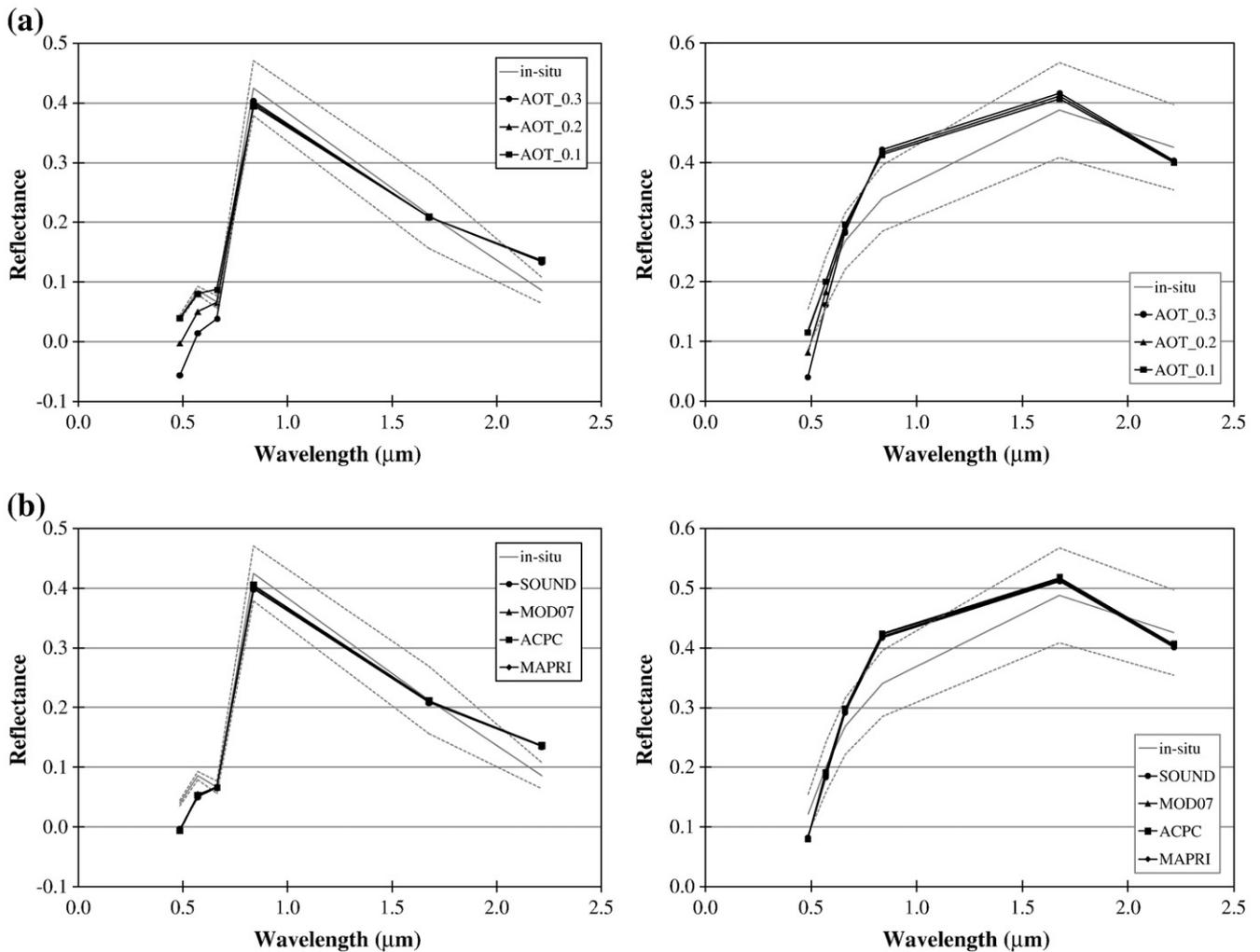
Fig. 9. Surface reflectance retrievals from Landsat5/TM data acquired on 13th July 2005 over festuca (left column) and bare soil (right column). (a) Comparison between retrievals using local sounding for atmospheric correction and different Aerosol Optical Thickness (AOT) at 550 nm values (0.1, 0.2 and 0.3) and the spectrum measured in-situ. (b) Comparison between retrievals using the different atmospheric profiles for an AOT content fixed at 0.2 and the spectrum measured in-situ.

(a)

(b)

(c)
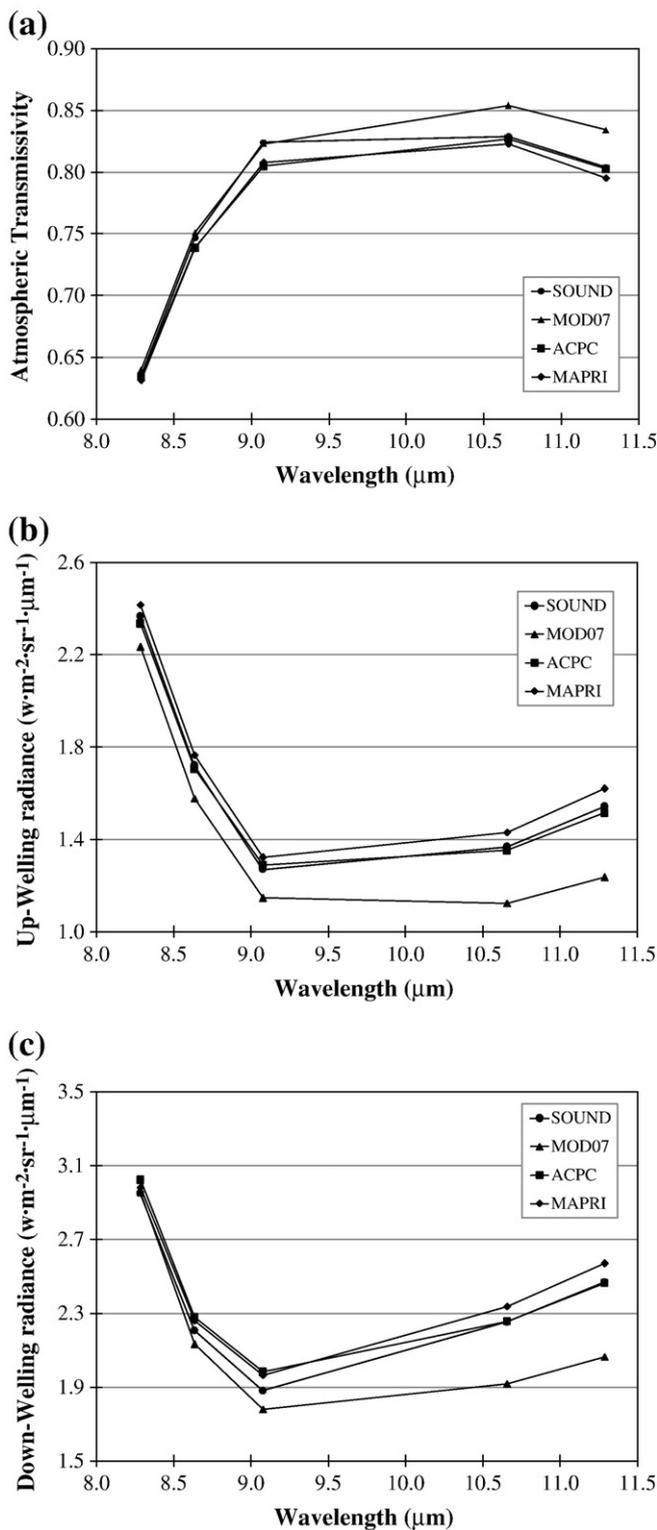
Fig. 10. Values of (a) transmissivity, (b) up-welling atmospheric radiance and (c) down-welling atmospheric radiance obtained from the different atmospheric profiles for ASTER TIR bands and for the test date 18th July 2004.

MAPRI provided a good agreement with SOUND. Table 3 includes basic statistics, with RMSE values of 2.3%, 13.8% and 10.8%, for τ, $L^\downarrow$, and $L^\uparrow$, respectively, and similar RMSE values for ACPC (1.3, 1.5 and 3.2%) and MAPRI (1.2, 3.9 and 3.5%).

Results in terms of LST and emissivity are provided in Table 4. Taking SOUND data as a reference, differences in LST when using MOD07, ACPC and MAPRI were 0.7, 0.3 and 0.3 K, respectively. Note

Table 3
Relative errors (in %) on ASTER atmospheric parameters obtained in the intercomparison between the different atmospheric profiles extracted on 18th July 2004 (SPARC), using local soundings as a reference.

		MOD07-SOUND	ACPC-SOUND	MAPRI-SOUND
τ	Band 10	0.8	−0.1	−0.6
	Band 11	0.5	−1.2	−1.2
	Band 12	−0.2	−2.4	−2.0
	Band 13	3.1	−0.2	−0.7
	Band 14	3.7	−0.2	−1.1
	BIAS	1.6	−0.8	−1.1
	STDEV	1.7	1.0	0.6
	RMSE	2.3	1.3	1.2
$L^\uparrow$	Band 10	−5.7	−1.4	2.1
	Band 11	−8.3	−0.9	2.6
	Band 12	−9.8	1.4	4.1
	Band 13	−17.8	−1.1	4.6
	Band 14	−19.9	−1.8	5.0
	BIAS	−12.3	−0.7	3.7
	STDEV	6.2	1.3	1.3
	RMSE	13.8	1.5	3.9
$L^\downarrow$	Band 10	0.1	2.4	1.0
	Band 11	−3.5	3.3	2.4
	Band 12	−5.3	5.4	4.4
	Band 13	−14.8	0.2	3.8
	Band 14	−16.4	−0.2	4.1
	BIAS	−8.0	2.2	3.2
	STDEV	7.2	2.3	1.4
	RMSE	10.8	3.2	3.5

that the significant differences found in the vertical profiles and the atmospheric parameters in 2004 only imply a difference in LST of a few tenths of degree. However, differences on emissivity are more notable, especially for ASTER bands 10, 11 and 12, with RMSE values between 1.5% and 4%. Acceptable differences were found for bands 13 and 14, below 1%.

7.2.2. TM (13 July 2005)

Atmospheric parameters for TM band 6 are presented in Table 5. In this case, contrary to the 2004 case, MOD07 provided the best agreement with SOUND (errors of −1.1, 2.3 and 4.1% for τ, $L^\downarrow$, and $L^\uparrow$ respectively), and MAPRI the highest differences (−11.1, 63.6 and 57.5%). Significant differences were found also for ACPC (−7.8, 33.1 and 32%). MOD07, ACPC and MAPRI profiles provided an underestimation of the atmospheric transmissivity, thus providing an overestimation in the atmospheric radiances.

Table 4
Comparison between Land Surface Temperature and Emissivity retrievals from TES algorithm using atmospheric parameters retrieved from MODTRAN4 code using the different atmospheric profiles (local sounding used as a reference) for the SPARC (18 July 2004) test case.

	Parameter	Min.	Max.	BIAS	STDEV	RMSE
MOD07-SOUND	ε_{10} (8.28 μm)	−0.025	0.038	0.025	0.009	0.027
	ε_{11} (8.64 μm)	−0.014	0.042	0.030	0.008	0.031
	ε_{12} (9.07 μm)	−0.003	0.051	0.039	0.007	0.040
	ε_{13} (10.66 μm)	−0.030	0.015	0.005	0.006	0.008
	ε_{14} (11.27 μm)	−0.025	0.019	0.008	0.006	0.010
	LST (K)	−1.3	1.8	−0.6	0.5	0.7
ACPC-SOUND	ε_{10} (8.28 μm)	−0.043	0.018	0.007	0.005	0.009
	ε_{11} (8.64 μm)	−0.023	0.032	0.021	0.005	0.021
	ε_{12} (9.07 μm)	−0.004	0.048	0.036	0.005	0.037
	ε_{13} (10.66 μm)	−0.031	0.014	0.005	0.004	0.006
	ε_{14} (11.27 μm)	−0.028	0.017	0.007	0.004	0.008
	LST (K)	−0.6	2.3	0.0	0.3	0.3
MAPRI-SOUND	ε_{10} (8.28 μm)	−0.041	0.012	0.003	0.004	0.005
	ε_{11} (8.64 μm)	−0.022	0.025	0.017	0.004	0.017
	ε_{12} (9.07 μm)	−0.004	0.040	0.032	0.004	0.032
	ε_{13} (10.66 μm)	−0.029	0.011	0.004	0.003	0.005
	ε_{14} (11.27 μm)	−0.027	0.013	0.006	0.003	0.007
	LST (K)	−0.6	1.8	−0.2	0.2	0.3

Table 5
Relative errors (in %) on Landsat5/TM atmospheric parameters obtained in the intercomparison between the different atmospheric profiles using local soundings as a reference for the 13th July 2005.

Parameter	MOD07-SOUND	ACPC-SOUND	MAPRI-SOUND
τ	−1.1	−7.8	−11.1
$L^{\uparrow}$	2.3	33.1	63.6
$L^{\downarrow}$	4.1	32.0	57.5

In terms of LST retrieval (Table 6), results were similar for MOD07 and MAPRI, with bias of (0.6 ± 0.1) K and (0.6 ± 0.7) K, respectively. In the case of ACPC, the mean difference was notably higher, with (1.9 ± 0.5) K. Since all bias values were positive, MOD07, ACPC and MAPRI overestimated the LST. It should be noted that in this case the huge differences found in the atmospheric parameters obtained from MAPRI and SOUND (see Table 5) are not reflected in the LST retrievals, which could be explained due to a compensation between errors (high negative difference in τ and high but positive difference in $L^{\downarrow}$ and $L^{\uparrow}$). In the case of ACPC, difference for τ is also negative, and differences for $L^{\downarrow}$ and $L^{\uparrow}$ also positive, but the magnitude of the errors are lower. Hence, errors in transmissivity between ACPC and MAPRI are similar (−8 and −11%, respectively), but errors on atmospheric radiances ($L^{\uparrow}$ and $L^{\downarrow}$) are almost doubled (around 30% versus 60%), which provokes a miscompensation of errors in the case of ACPC (Table 6).

8. Summary and conclusions

In this paper we discussed the feasibility of using different sources of atmospheric profiles for atmospheric corrections in the optical region covering VNIR, SWIR and TIR. The Mid Infra-Red (MIR) region was excluded in the analysis, since it requires additional work due to the contribution of both solar and emission terms during daytime. At nighttime, RTE in the MIR is equivalent to the TIR one. For this purpose, MODIS (MOD07) and Reanalysis-based atmospheric profiles products were used. Regarding Reanalysis information, one existing product was considered (ACPC), and other improved product was created (MAPRI). All the three products (MOD07, ACPC and MAPRI) were compared to local soundings (considered as a ground-truth) at three test dates (12th July 2003, 18th July 2004 and 13th July 2005) and differences on the atmospheric correction of optical imagery acquired with CHRIS, ASTER and TM sensors over an agricultural area in Spain were assessed.

In general terms, and despite significant differences were found in the vertical distribution of dew point temperatures (but similar profiles were observed in the case of air temperature), every atmospheric profile analyzed provided a useful tool for accurate atmospheric correction of optical imagery in those cases where a local sounding is not available. In the case of the visible region the main input parameter for accurate AC is the AOT, and not the atmospheric profile itself. This parameter was extracted from MOD04 product, and an overestimation of near to 0.1 was detected in comparison to in-situ measurements in 2003 and 2004 test cases. The overestimation was lower in 2005, only 0.04. Those overestimations provoked an

Table 6
Comparison between Land Surface Temperature retrievals from Single-Channel algorithm using atmospheric parameters retrieved from MODTRAN4 code using the different atmospheric profiles (local sounding used as a reference) for the SEN2FLEX (13 July 2005) test case.

	Min. (K)	Max. (K)	BIAS (K)	STDEV (K)	RMSE (K)
MOD07-SOUND	0.5	0.7	0.6	0.1	0.6
ACPC-SOUND	0.8	2.7	1.9	0.5	2.0
MAPRI-SOUND	−1.3	1.8	0.6	0.7	0.9

underestimation on the retrieved surface reflectances, so it is important to correct the bias of the MOD04 product in order to use it for AC purposes (alternatively image-based method can be used). In the SWIR region the main parameter to be controlled is the atmospheric water vapor content (which can be different due to a different atmospheric profile) more than the AOT, but the effect of water vapor in the SWIR is lower than the AOT effect in the visible. Water vapor effect is more notable for narrow-bands in the SWIR, as is the case of ASTER, than for broader bands, as is the case of TM. The NIR region around 0.8 μm is almost insensitive to both AOT and water vapor. Therefore, as a conclusion of the results obtained in the test cases analyzed in this paper, we can say that all the three MOD07, ACPC and MAPRI profiles are equally valid for AC in the VNIR–SWIR region whenever an accurate estimation of AOT is available.

In the TIR region, since aerosols are not accounted for, the main atmospheric constituent involved in the AC is the water vapor content, so differences on the atmospheric profiles are more critical than in the VNIR–SWIR case. In the 2004 test case, in which an ASTER image was used, MOD07 provided the highest differences in comparison to the atmospheric parameters (τ, $L^{\downarrow}$, and $L^{\uparrow}$) retrieved from the local sounding, whereas ACPC and MAPRI provided results similar to the local sounding. The differences found when using the MOD07 product were not dramatically translated in the LST retrieval, since a RMSE value of 0.7 K was obtained when compared to the use of local sounding. In the ACPC and MAPRI cases, RMSE values were only 0.3 K in both cases. Low differences on emissivity (<1%) at ASTER bands 13 and 14 (located between 10 and 12 μm) were found for all the three products, but differences ranged between 2 and 4% for bands 10, 11 and 12 located in the 8–9 μm spectral region. However, in the 2005 test case, in which a Landsat5/TM image was used, MOD07 provided the best agreement with the local sounding and MAPRI provided the highest differences, with ACPC providing also significant differences. In terms of LST retrieval, MOD07 provided a RMSE of 0.6 K when compared to the local sounding. The huge differences found when using the MAPRI product were not reflected in LST retrievals, since a RMSE of 0.9 K (when compared to the use of the local sounding) was obtained. This is attributed to compensation between errors, in which underestimations on transmissivity are compensated by overestimations on atmospheric radiances. This compensation was not found in the ACPC case, with a RMSE of 2 K, because the error on the atmospheric radiances were significantly lower than in the MAPRI case, but the error on the transmissivity was similar. A different behavior for TM band 6 in comparison to ASTER TIR bands was also found due to different band-width (around 0.5 and 0.75 μm for ASTER and 2 μm for TM). Therefore, for the test cases analyzed for AC in the TIR, MOD07 and MAPRI provided satisfactory results, and they demonstrated to be a useful source for AC in this spectral region. ACPC results were accurate in 2004 but not as accurate in 2005, but still acceptable in terms of errors for LST retrievals over land. The main advantage of MOD07 product is its high spatial resolution (5 km), but it is only available from year 2000, whereas MAPRI provides a lower spatial resolution but it can be used for AC of historical databases of satellite imagery (since it is available at least from 1970 to present). At this moment, ACPC profiles included in the web-based tool are only available from 2000, and results are sent by mail to the user, which somehow jeopardizes its operational use.

Note that the results presented in this paper refer to agricultural areas and mid-latitude summer conditions, with atmospheric water vapor contents around 2 g/cm². Further analysis is required to extract conclusions over other environments and atmospheric conditions.

References

Barsi, J. A., Barker, J. L., & Schott, J. R. (2003). *An Atmospheric Correction Parameter Calculator for a single thermal band earth-sensing instrument.* Toulouse, France: IGARSS IEEE International Geoscience and Remote Sensing Symposium.

Barsi, J. A., Schott, J. R., Palluconi, F. D., & Hook, S. J. (2005). *Validation of a Web-Based Atmospheric Correction Tool for Single Thermal Band InstrumentsProceedings of SPIE, vol. 5882*, Bellingham, WA.

Berk, A., Anderson, G. P., Acharya, P. K., Chetwynd, J. H., Bernstein, L. S., Shettle, E. P., et al. (1999). *MODTRAN4 User's Manual.* Hanscom AFB, MA: Air Force Research Laboratory.

Cristóbal, J., Jiménez-Muñoz, J. C., Sobrino, J. A., Ninyerola, M., & Pons, X. (2009). Improvements in land surface temperature retrieval from the Landsat series thermal band using water vapor and air temperature. *Journal of Geophysical Research, 114*, D08103, doi:10.1029/2008JD010616.

Delbart, N., Picard, G., Le Toan, T., Kergoat, L., Quegan, S., Woodward, I., et al. (2008). Spring phenology in boreal Eurasia in a nearly century time-scale. *Global Change Biology, 14*(3), 603−614.

Estellés, V., Molero, F., Gómez-Amo, J. L., Fortea, J. C., Pedrós, R., Utrillas, M. P., et al. (2008). Characterization of the atmosphere during SEN2FLEX 2005 field campaign. *Journal of Geophysical Research, 113*, D09205, doi:10.1029/2007JD009237.

Gillespie, A., Rokugawa, S., Matsunaga, T., Cothern, J. S., Hook, S., & Kahle, A. B. (1998). A temperature and emissivity separation algorithm for advanced spaceborne thermal emission and reflection radiometer (ASTER) images. *IEEE Transactions on Geoscience and Remote Sensing, 36*(4), 1113−1126.

Guanter, L., Alonso, L., & Moreno, J. (2005). A method for the surface reflectance retrieval from PROBA/CHRIS data over land: Application to ESA SPARC campaigns. *IEEE Transactions on Geoscience and Remote Sensing, 43*(12), 2908−2917.

Guanter, L., Richter, R., & Kaufmann, H. (2009). On the application of the MODTRAN4 atmospheric radiative transfer code to optical remote sensing. *International Journal of Remote Sensing, 30*(6), 1407−1424.

Jiménez-Muñoz, J. C., & Sobrino, J. A. (2003). A generalized single-channel method for retrieving land surface temperature from remote sensing data. *Journal of Geophysical Research, 108*, D22, doi:10.1029/2003JD003480.

Jiménez-Muñoz, J. C., & Sobrino, J. A. (2007). Feasibility of retrieving land-surface temperature from ASTER TIR band using two-channel algorithms: A case study of agricultural areas. *IEEE Geoscience and Remote Sensing Letters, 4*(1), 60−64.

Jiménez-Muñoz, J. C., & Sobrino, J. A. (2009). A single-channel algorithm for land-surface temperature retrieval from ASTER data. *IEEE Geoscience and Remote Sensing Letters, 7*(1), 176–179.

Jiménez-Muñoz, J. C., Cristóbal, J., Sobrino, J. A., Sòria, G., Ninyerola, M., & Pons, X. (2009). Revision of the single-channel algorithm for land surface temperature retrieval from Landsat thermal-infrared data. *IEEE Transactions on Geoscience and Remote Sensing, 47*(1), 339−349.

Jiménez-Muñoz, J. C., Sobrino, J. A., Plaza, A., Guanter, L., Moreno, J., & Martínez, P. (2009). Comparison between fractional vegetation cover retrievals from vegetation indices and spectral mixture analysis: Case study of PROBA/CHRIS data over an agricultural area. *Sensors, 9*, 768−793.

Kalnay, E., Kanamitsu, M., Kistler, R., Collins, W., Deaven, D., Gandin, L., et al. (1996). The NCEP/NCAR 40-year reanalysis project. *Bulletin of the American Meteorological Society, 77*, 437−470.

Kistler, R., Collins, W., Saha, S., White, G., Woollen, J., Kalnay, E., et al. (2001). The NCEP-NCAR 50-year reanalysis: Monthly means CD-ROM and documentation. *Bulletin of the American Meteorological Society, 82*, 247−267.

Lary, D. J., Remer, L. A., MacNeill, D., Roscoe, B., & Paradise, S. (2009). Machine learning and bias correction of MODIS aerosol optical depth. *IEEE Geoscience and Remote Sensing Letters, 6*(4), 694−698.

Levy, R. C., Remer, L. A., Martins, J. V., & Kaufman, Y. J. (2005). Evaluation of the MODIS aerosol retrievals over ocean and land during CLAMS. *Journal of Atmospheric Sciences, 62*, 974−992.

Molero, F., Pujadas, M., Fortea, J. C., Gómez-Amo, J. L., Estellés, V., Utrillas, M. P., et al. (2005). Vertical profiles of atmospheric constituents from LIDAR and sounding measurements. *Proceedings of the SPARC Final Workshop, 4–5 July, ITC, Enschede, The Netherlands.*

Molero, F., Estellés, V., Pujadas, M., Martínez-Lozano, J. A., Fortea, J. C., Gómez-Amo, J. L., et al. (2006). Characterization of the atmosphere in the Sen2Flex campaign: Ground based measurements of columnar and vertically-resolved atmospheric constituents, Sentinel-2 and flourescence experiment. *Proceedings of the SEN2FLEX Final Workshop, 30–31 October, ESA/ESTEC, Noordwijk, The Netherlands.*

Moreno, J., Caselles, V., Martínez-Lozano, J. A., Meliá, J., Sobrino, J. A., Calera, A., et al. (2001). The measurements programme at Barrax. *DAISEX Final Results Workshop, ESTEC, Holland, 15–16 March, ESA Publications Division, SP-499* (pp. 43−51).

Moreno, J., Alonso, L., Fernández, G., Fortea, J. C., Gandía, S., Guanter, L., et al. (2004). The SPECTRA Barrax Campaign (SPARC): Overview and first results from CHRIS data. *Proceedings of 2nd CHRIS/PROBA Workshop, Frascati, Italy, ESA-ESRIN.*

Ngo-Duc, T., Polcher, J., & Laval, K. (2005). A 53-year forcing data set for land surface models. *Journal of Geophysical Research, 110*, D06116, doi:10.1029/2004JD005434.

Papadimas, C. D., Mihalopoulos, N., Kanakidou, M., Katsoulis, B. D., & Vardavas, I. (2008). Assessment of the MODIS Collections C005 and C004 aerosol optical depth products over the Mediterranean basin. *Atmospheric Chemistry and Physics Discussions, 8*, 16891−16916.

Seemann, S. W., Borbas, E. E., Li, J., Menzel, W. P., & Gumley, L. E. (2006). *"MODIS atmospheric profile retrieval algorithm theoretical basis document.* version 6, October 25.

Sobrino, J. A., Julien, Y., & Morales, L. (2006). Multitemporal analysis of PAL images for the study of land cover dynamics in South America. *Global and Planetary Change, 51*, 172−180.

Sobrino, J. A., Jiménez-Muñoz, J. C., Balick, L., Gillespie, A., Sabol, D., & Gustafson, W. T. (2007). Accuracy of ASTER Level-2 thermal-infrared standard products of an agricultural area in Spain. *Remote Sensing of Environment, 106*(2), 146−153.

Sobrino, J. A., Mattar, C., Pardo, P., Jiménez-Muñoz, J. C., Hook, S. J., Baldridge, A., et al. (2009). Soil emissivity and reflectance spectra measurements. *Applied Optics, 48* (19), 3664−3670.

Stamnes, K., Tsay, S. C., Wiscombe, W., & Jayaweera, K. (1988). Numerically stable algorithm for discrete–ordinate-method radiative transfer in multiple scattering and emitting layered media. *Applied Optics, 27*(12), 2502−2509.

Verhoef, W., & Bach, H. (2003). Simulation of hyperspectral and directional radiance images using biophysical and atmospheric radiative transfer models. *Remote Sensing of Environment, 87*, 23−41.